Available online at www.eccomasproceedia.org
Eccomas Proceedia COMPDYN (2017) 595-612

ECCOMAS
Proceedia

COMPDYN 2017
6th ECCOMAS Thematic Conference on
Computational Methods in Structural Dynamics and Earthquake Engineering
M. Papadrakakis, M. Fragiadakis (eds.)
Rhodes Island, Greece, 15–17 June 2017

SEISMIC CAPACITY AND DEMAND ASSESSMENT IN BRIDGE-SPECIFIC FRAGILITY ANALYSIS

Sotiria P. Stefanidou[1] **and Andreas J. Kappos**[2]

[1] Department of Civil Engineering, Aristotle University
Thessaloniki, 54124, Greece
e-mail: ssotiria@civil.auth.gr

[2] Department of Civil Engineering, City, University of London
London EC1V OHB, UK
e-mail: Andreas.Kappos.1@city.ac.uk

Keywords: Bridges, Seismic Demand, Fragility Curves, Nonlinear Analysis

Abstract. *During the last three decades, a large number of analytical methodologies have been developed for the seismic assessment of bridges and the derivation of bridge fragility curves. However, recently, the research focus has shifted on the derivation of bridge-specific fragility curves, recognizing the effect of different geometry, structural system, component and soil properties, on the seismic assessment results. In this context, a new, component-based methodology for the derivation of bridge-specific fragility curves has been proposed by the authors, with a view to overcoming the inherent difficulties in assessing all bridges of a road network and the drawbacks of existing methodologies, which propose usage of the same group of fragility curves for bridges classified within the same category. Therefore, the main issue addressed in this paper is to analytically determine capacity and demand in bridge-specific fragility analysis in the frame of the methodology previously proposed by the authors, aiming at application to realistically sized bridge stocks. Capacity (resistance) is calculated individually for each critical component with the aid of inelastic pushover analysis, quantifying damage in displacement terms based on the capacity curve and the correlation of global to local damage. Bridge piers, abutments and bearings are considered as the (seismically) critical components of a bridge system; piers of different types and characteristics, and different types of abutments and bearings are analysed and included in a database that provides case-specific limit state thresholds of component capacity. The effect of component parameters on limit state thresholds is therefore assessed, highlighting the differences according to the limit state and component considered. Demand is also calculated for each component using either inelastic response-history or elastic dynamic analysis, depending on the application scale (single bridge vs bridge stock), while uncertainties in both capacity and demand are quantified. Case-specific capacity and demand estimations using the proposed methodology are given here for three bridges having different structural systems, and the derived bridge-specific fragility curves are compared with fragility curves for all bridges classified within the same category, to assess the degree of over- or under- estimation of the probability of damage when generic bridge classes are used.*

Peer-review under responsibility of the organizing committee of COMPDYN 2017.
doi: 10.7712/120117.5443.17921

1 INTRODUCTION

Reliability of road systems and their components, exposed to multiple natural hazards is on the frontline of engineering research during the last three decades, since possible damage to critical components is strongly related to important direct and indirect economic losses. Bridges are considered to be the most critical component of urban and interurban transportation systems, ensuring mobility and intercity connection after an earthquake event. Therefore, numerous methods have been developed for the assessment of seismic vulnerability of bridges, mainly in the context of developing fragility curves.

Seismic fragility is the quantification of the probability that bridge damage will exceed a specific limit state threshold for a given level of earthquake intensity. Fragility curves are derived for different limit states and levels of earthquake intensity and can be used for pre-earthquake retrofit prioritization. The majority of the methodologies available in the literature for the derivation of fragility curves are analytical, since earthquake damage data available to derive empirical bridge fragility curves is sparse. A great number of analytical methodologies is available in the literature (Table 1), and can be classified with regard to consideration of multiple components ([1], [2], [3], [4], [5], [6]), or only the most critical one (piers) in fragility analysis, the estimation of component or system capacity (limit state thresholds) and seismic demand (analysis method used), the uncertainty treatment and the probabilistic model used. In particular, regarding component capacity, either local ([5], [6], [7]), or global ([8], [9]) engineering demand parameters are used, whereas quantification of damage, namely the limit state thresholds, is commonly based on experimental results ([10], [11], [12]). Regarding the calculation of seismic demand, different analysis methods have been put forward, namely inelastic static (pushover) analysis (e.g. [3], [4]), modal response spectrum method (e.g. [1], [12]??), and nonlinear response-history analysis ([13], [14]). The maximum likelihood method [15] or the probabilistic seismic demand model ([2], [16]) have been used for the calculation of fragility curves.

The variability in capacity and demand estimation in the frame of analytical methodologies for the derivation of fragility curves is depicted in Table 1. The main drawback of the existing methodologies is that capacity (limit state threshold) estimation is commonly based on experimental results ignoring the effect of structure-specific parameters like pier type, geometry, material, and reinforcement properties on results, whereas advanced analysis tools are proposed for the estimation of seismic demand, increasing the computational cost when applied to large bridge inventories. A new, component based methodology for the derivation of bridge-specific fragility curves has been recently proposed by the authors [17], having a broad application range (the method is independent of the structural system and the bridge properties), and being feasible to be applied to realistically sized bridge stocks. The main issue addressed in this paper is to analytically determine the capacity of multiple bridge components, providing component-specific limit state thresholds and closed-form equations for their quantification, while the effect of different pier type and properties on local and global engineering demand parameters is assessed and discussed. Moreover, the estimation of seismic demand from the analysis of a detailed or simplified model depending on the application scale (single bridge or bridge stocks) in the frame of bridge-specific analysis is presented and discussed. Finally, bridge-specific fragility curves derived for three bridges are compared with fragility curves for the corresponding generic bridges, to assess the degree of over- or under- estimation of the probability of damage when generic bridge classes are used.

Research Group	Capacity		Seismic Demand		
	Engineering Demand Parameter	**Limit State thresholds**	**Structural model**	**Seismic Input**	**Analysis Method**
1. Avşar *et al.* (2011)	Piers: φ Beams: φ, V_u Bearings: δ [3 LS]	*Piers:* Priestley *et al.*, (1996), Erduran & Yakut, (2004) *Bearings:* FHWA, (2006)	3D DM	25 accel. (no scaling)	NRHA
2. Banerjee & Shinozuka (2007)	Piers: μ_θ [5 LS]	Dutta, (1999)	3D DM	3 × 20 accel.	NRHA & CSM
3. Cardone, Perrone, & Dolce (2007), Cardone (2013)	Piers: δ Bearings: δ Abutments: δ [5 LS]	*Piers:* δ_y & δ_u *Bearings:* γ (%) Konstantinidis et al. (2008) *Abutments:* δ_{gap} & δ_u	MDOF→SDOF, Adaptive Pushover	Spectrum	CSM (adaptive)
4. Choi *et al.* (2004)	Piers: μ_φ Bearings: δ [5 LS]	*Piers:* Dutta, (1999) *Bearings:* Experiments	3D DM	100 synthetic accel.	NRHA
5. Crowley *et al.* (2011), Tsionis & Fardis (2012)	Piers: θ Bearings: δ [2 LS]	*Piers:* θ_y & θ_u Biskinis & Fardis, (2010a, b) *Bearings:* Bousias *et al.* 2007	SDOF*(Long)*, Beam with springs (*Trans*)	EC8 elastic spectrum	Equivalent Static
6. De Felice & Giannini (2010)	Piers: θ [2 LS]	θ_y & θ_u	Metamodels	2 ×4 accel.	NRHA - RSM
7. Dukes (2013)	Piers: μ_φ Bearings: δ Abutments: δ [4 LS]	*Piers:* Dutta, (1999) *Bearings - Abutments*: Caltrans (2010)	Metamodels	3 ×40 accel.	NRHA - RSM
8. Elnashai *et al.* (2004)	Piers: δ	δ_y & δ_u (Pushover Curve)	3D DM	7accel. (scaled)	NRHA
9. Ghosh *et al.* (2013)	Piers: μ_φ Bearings: δ Abutments: δ [4 LS]	Nielson & DesRoches (2007)	Metamodels	24 accel. (Wen& Wu)	NRHA - RSM
10. Hwang *et al.*, (2001)	Piers: *C/D factors or* μ_δ [5 LS]	*Piers:* δ_y & δ_u	3D DM	100 acc. synthetic	NRHA
11. Karim & Yamazaki (2001,2003)	DI=(μ_δ+$\beta\mu_h$)/μ_u (Park-Ang) [5 LS]	*DI*=0.00~1.00	SDOF	250 accel.	Nonlinear Static/NRHA
12. Mackie & Stojadinović (2004)	Drift (%)	Berry & Eberhard (2003)	3D DM	80 accel.	NRHA
13. Mander & Basöz (1999)	Piers: *δ/h (%)* Bearings: δ [5 LS]	Dutta, (1999)	SDOF	Elastic spectrum	CSM
14. Moschonas *et al.* (2008)	Bridge: δ [5 LS] [5 LS]	*Piers:* δ_y & δ_u (Pushover curve) *Bearings:* δ (γ %)	3D DM	Elastic spectrum	CSM
15. Nielson & DesRoches (2007a, b)	Piers: μ_φ Bearings: δ Abutments: δ [4 LS]	*Piers:* HAZUS (1997), FHWA (2006) *Bearings*, *Abutments* : Choi (2004)	3D DM	48 accel. (3 bins)	NRHA
16. Ramanathan, (2012)	Piers: μ_φ Bearings: δ Abutments: δ [4 LS]	*Piers:* Berry & Eberhard (2003), *Bearings*, *Abutments* : Caltrans (2010)	3D DM	320 accel. (4 bins)	NRHA
17. Shinozuka *et al.*	Piers: μ_δ [3 LS]	$1.0 \le \mu_\delta \le 2.0$	3D DM	80 accel.	NRHA

(2000)					
18. Tavares *et al.*, (2012)	Piers: μ_φ Bearings: δ Abutments: δ [4 LS]	HAZUS (1997)	3D DM	Synthet-ic Accel.	NRHA
19. Yi *et al.* (2007)	Piers: μ_φ Bearings: δ	Choi (2004)	2D Model	60 accel.	NRHA
20. Zhong *et al.* (2012)	Piers: Drift (%)	Probabilistic model (closed form relationship)	3D DM	Elastic spectrum	CSM

* ***3D DM:*** 3D Detailed Model, ***NRHA***: Nonlinear Response History Analysis ***CSM***: Capacity Spectrum Method

Table 1: Capacity and demand estimation in analytical methodologies for the derivation of fragility curves (full references provided in [18]

2 METHODOLOGY FOR DERIVING BRIDGE-SPECIFIC FRAGILITY CURVES

The methodology, proposed by the authors, for the derivation of bridge-specific fragility curves and the distinct steps for its implementation are described in detail elsewhere [17]. It is noted that a key aspect of the methodology is the broad application range, independently of the structural system and bridge properties, in principle overcoming the need for classification to typological classes. The methodology is component-based and provides closed-form relationships for the quantification of component-specific limit state thresholds (component database) and two alternatives for the calculation of seismic demand based on analysis of a detailed or simplified bridge model, depending on whether a single bridge or bridge stock is addressed. A detailed description of the methodology is beyond the scope of this paper, however basic principles for the estimation of component capacity (database development) and seismic demand are briefly described in the remainder of this section.

2.1 Bridge capacity

As depicted in Table 1, different global or local engineering demand parameters are proposed by methodologies available in the literature for the quantification of component damage, while threshold values are based on experimental results in most cases. Analytical estimation of limit state thresholds is rarely proposed, whereas component-specific analysis is required in that case, rendering the methodology case-dependent and simultaneously increasing the computational cost.

In the frame of the proposed methodology, bridge piers, abutments and bearings are considered as critical components affecting the system's seismic performance and limit state thresholds for four limit states are explicitly defined based on inelastic analysis results and/or experimental data, depending on the component examined. The milestone of the proposed methodology regarding the capacity estimation, is that the user- can define component limit state thresholds for four limit states considering all different component properties that may affect inelastic behaviour based on analysis results, without performing inelastic analysis for each component. To this end, a database of different components is developed and multiple parametric analyses are performed, to obtain limit state thresholds based on inelastic analysis results, additionally considering different possible failure modes. Based on regression analysis of results, closed-form relationships are provided for limit state thresholds, based on various parameters affecting capacity for different component types. Therefore, irrespectively of the methodology followed for fragility estimation, a reliable methodology for limit state threshold (capacity) estimation is provided.

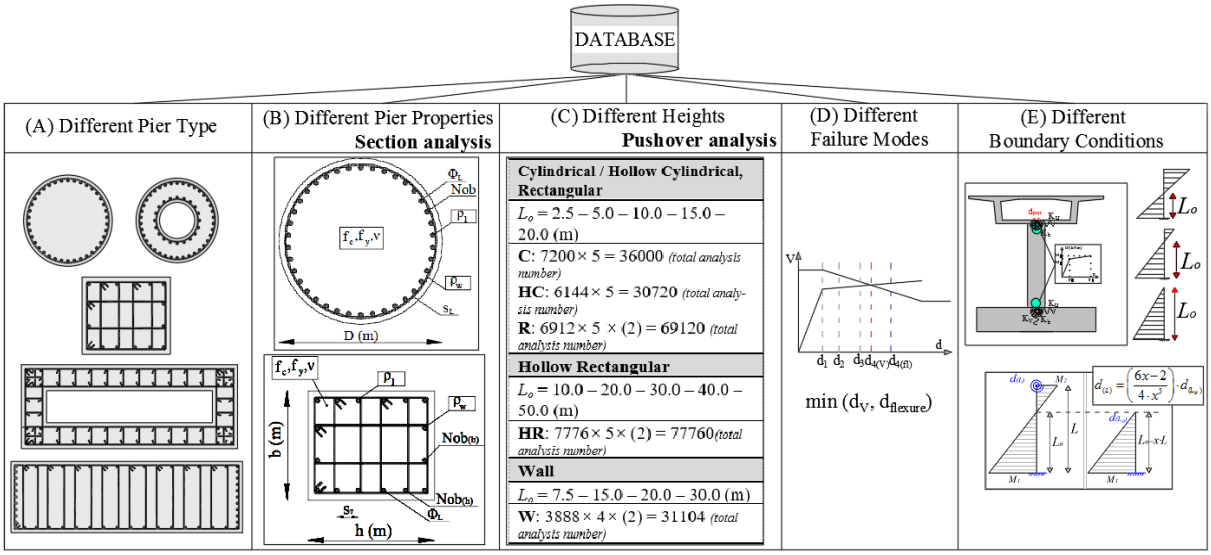

Fig. 1 – Development of database for bridge piers

Regarding the component which is usually the most critical for the seismic response, namely bridge piers, the procedure followed for the development of the database is presented in Fig. 1. The distinct steps for the compilation of database are:

(a) Consideration of different pier types, encompassing practically all different types found in a bridge stock. Cylindrical, hollow cylindrical, rectangular, hollow rectangular and wall piers are considered herein. It should be mentioned that hollow rectangular and wall piers are commonly designed to remain elastic (in bridges with pier-to-deck connection through bearings), however their inelastic behaviour is additionally studied and limit state thresholds are quantified.

(b) Consideration of varying pier section parameters, namely dimensions, longitudinal and transverse reinforcement ratio, normalised axial force and material properties. Section analyses are performed for all possible combinations of parameters considering confined and unconfined concrete material laws. In particular, regarding confined concrete, the Mander model [19] was used for cylindrical sections, Priestley & Ranzo model [20] for hollow cylindrical, and Kappos model [21] for rectangular, hollow rectangular, and wall sections. Parametrically defined input cross section files are set up and multiple section analyses are performed using AnySection v.4.2.0 [22]. Pier damage is initially defined at section level, using local engineering demand parameters (section curvature), related to experimentally estimated damage (e.g. crack widths) via section analysis, therefore limit state thresholds in curvature (local) terms (Table 1) are defined within this step.

(c) Consideration of a sufficiently broad range of heights for each pier section type and parametric setup of an inelastic cantilever model in order to perform pushover analysis and calculate limit state thresholds in terms of global engineering demand parameter (displacement of control point). Plastic hinge formation is considered at the cantilever base (lumped plasticity model), whereas M-φ curve, calculated at step (b), is used as input. Inelastic pushover analysis is performed for all sections considered (strong and weak section direction separately) paired with all different pier heights, using a Matlab-based code developed for the setup of input files, and Opensees [23] for inelastic static analysis. Limit state thresholds in *global* engineering terms (displacement of control point for limit states 1 to 4) are correlated to *local* ones (curvature for limit states 1 to

4), using the results of inelastic pushover analysis, additionally considering P-delta effects.

(d) Check of shear failure, calculating the displacement when V_u is developed (d_V), additionally considering reduced concrete contribution in the inelastic range (Fig.1). Displacement at shear failure (d_V) is compared to the displacement due to flexural failure (d_{fl}) and the minimum value is considered as threshold value for the specific limit state (Table 1).

Based on inelastic static analysis results, limit state thresholds are defined in displacement terms for all different pier types, section properties and heights considered (d_1 to d_4 for all possible combinations described within steps a-d), and regression analysis is performed in order to derive closed-form relationships for every pier type and limit state.

(e) Since all the previous steps are based on inelastic cantilever model and analysis results, the effect of different boundary conditions on limit state thresholds should also be considered. In general, bridge piers are restrained at the top (depending on the type of pier-to-deck connection and the type of the deck, namely deck rotational stiffness) and at the bottom, depending on the foundation type and the ground properties. The tip displacement of the equivalent cantilever (height equal to the height of contraflexure point calculated for each case as pier top to bottom moment ratio, from elastic analysis) is related to the displacement of the restrained pier, on the basis of the methodology described and the analytical solution provided in [17] and shown in Fig.1(E).

Limit State	R/C Piers / EDP: ***d* (m)**		Abutments EDP: ***d* (m)**	Bearings EDP: **γ (%)**
	Local	*Global*		
LS 1 – Minor/Slight damage	φ_1: φ_y	d_1: $\min\left\{\begin{matrix} d(\varphi_1) \\ d(\mathrm{V}_1) \end{matrix}\right\}$	$d_1 = 1.1 \cdot d_{gap}$ $(\mu_{\varphi,backwall} = 1.5)$	20 $(d_1 = 0.02 \cdot h_{br})$
LS 2 – Moderate damage	φ_2: min (φ: $\varepsilon_c > 0.004$, φ: $\varepsilon_s \geq 0.015$)	d_2: $\min\left\{\begin{matrix} d(\varphi_2) \\ d(\mathrm{V}_2) \end{matrix}\right\}$	$d_2 = 0.01 \cdot h_{backwall}$	100 $(d_2 = 0.1 \cdot h_{br})$
LS 3 – Major/Exten-sive damage	φ_3: min (φ: $\varepsilon_c \leq 0.004 + 1.4 \cdot \rho_w \cdot \frac{f_{yw}}{f_{cc}}$ φ: $\varepsilon_s \geq 0.06$)	d_3: $\min\left\{\begin{matrix} d(\varphi_3) \\ d(\mathrm{V}_3) \end{matrix}\right\}$	$d_3 = 0.035 \cdot h_{backwall}$	200 $(d_3 = 0.2 \cdot h_{br})$
LS 4 – Failure/Collapse	φ_4: min (φ: $M < 0.90 \cdot M_{\max}$, φ: $\varepsilon_s \geq 0.075$)	d_4: $\min\left\{\begin{matrix} d(\varphi_4) \\ d(\mathrm{V}_4) \end{matrix}\right\}$	$d_4 = 0.1 \cdot h_{backwall}$	300 $(d_4 = 0.3 \cdot h_{br})$

Table 1 – Limit state thresholds for critical structural components

For the quantification of abutment and bearing damage, threshold limit state values are defined in terms of displacement of the component control point, based on experimental results and other information from the literature, as described in [17] and summarised in Table 1.

In particular, threshold displacement values for abutments are related to the curvature ductility (LS1) and backwall height (LS2 to LS4). However, since curvature ductility is related to backwall inelastic performance and properties (M-φ curve), correlation to gap size is attempted in order to easily define threshold limit state value for LS1, avoiding inelastic analysis of the component in each application. To this end, parametric analyses of abutment (component)

models are performed, considering varying backwall heights and section properties as well as different backfill soil properties. Based on analyses results, the displacement corresponding to μ_φ=1.5 was approximately equal to 1.1d_{gap} (Table 1).

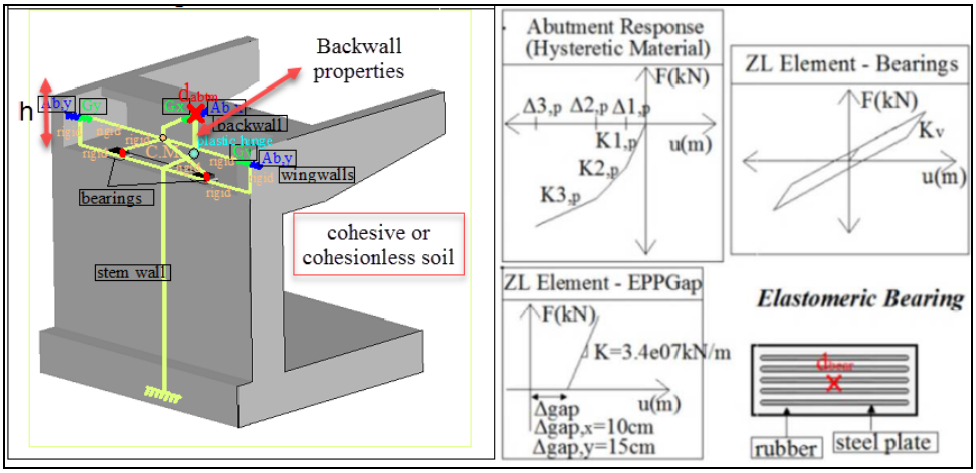

Fig. 2 – Stick model for the abutment

Threshold displacement values for elastomeric bearings are related to shear strain, based on experimental data (Table 1). For the case of lead rubber bearings, limit state thresholds are differentiated mainly regarding LS1, associated with the shear strain corresponding to lead core yielding. It should be noted that for both elastomeric and lead rubber bearings, attainment of the buckling load (P_{cr}) is also checked, whereas pot bearings, allowing sliding in one or both directions are not considered as critical components.

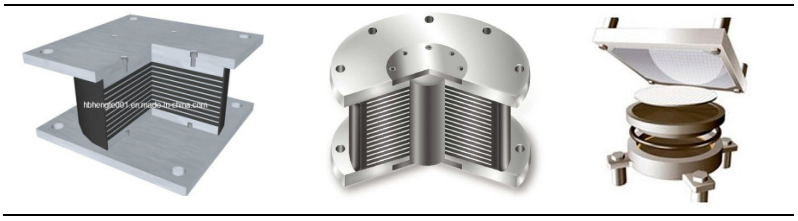

Fig. 3 – Elastomeric, lead rubber and pot bearings

Based on the above, a database of critical components is developed, providing component-specific limit state thresholds (as described in §3), for calculating component capacity (and the associated uncertainty β_c). A website providing all information regarding the database compilation, namely software developed for multiple parametric inelastic static component analysis and analytical limit state threshold definition, experimental data collected for quantitative damage definition, etc., is currently under development. The site will eventually provide an online platform, allowing component-specific limit state threshold quantification in the frame of fragility analysis, avoiding both time-consuming inelastic analyses and approximate definition of capacity regardless of the properties of the component , that will affect the reliability of fragility analysis.

2.2 Seismic demand

In the frame of the proposed methodology, the calculation of seismic demand at the component control point is differentiated depending on the application scale (single bridge or bridge stocks). In particular, when bridge-specific fragility curves are derived for a single

bridge, nonlinear response history analysis of a detailed inelastic model is proposed, using an enhanced IDA procedure described in [17] (IDA combined with multiple stripe analysis), in order to estimate seismic demand at component control points for different levels of earthquake intensity. Uncertainty in seismic demand (β_D) is calculated for every critical component, additionally considering the effect of record-to-record variability. Since the application of the methodology to bridge stocks for the derivation of bridge-specific fragility curves is computationally demanding, response spectrum analysis of a simplified elastic model for varying levels of earthquake intensity is proposed in this case (scaling PGA, e.g. from 0.1g to 1g) to estimate seismic demand at component control points, whereas the evolution of damage with earthquake intensity is plotted for every component considered (mean value). Bridge-specific fragility curves are plotted assuming lognormal distribution, while uncertainty in seismic demand (β_D), calculated for generic bridges representative of a specific bridge class according to the classification system presented in [24], is used as dispersion value.

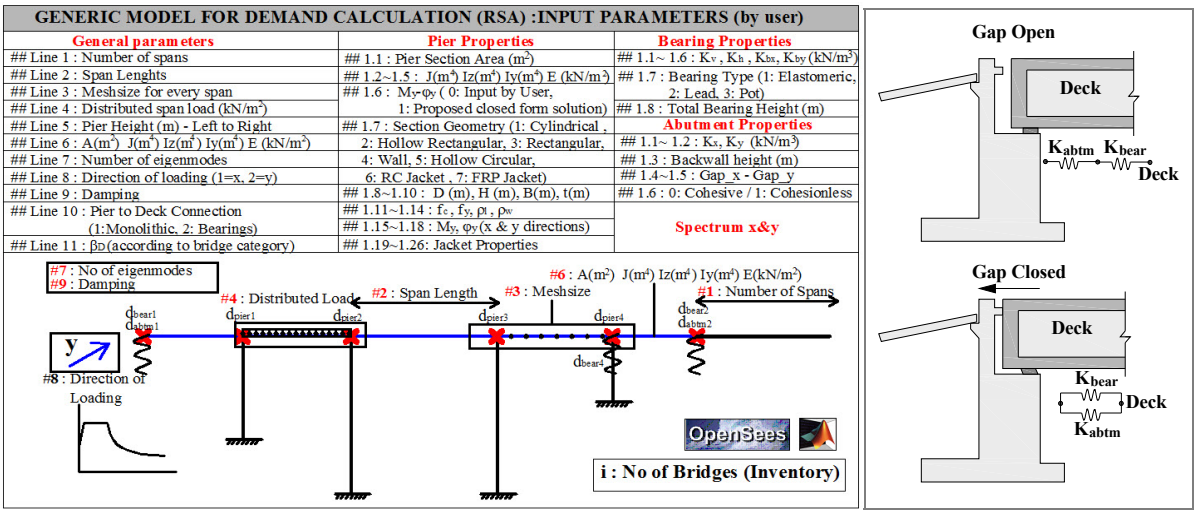

Fig. 4 – Software for bridge-specific fragility curves (input data – cases of open/closed gap)

The Matlab-based software developed for the implementation of the previously described methodology and the derivation of bridge-specific fragility curves is illustrated in Fig. 4. The software is based on a generic simplified 3D bridge model created using the OpenSees platform [23], wherein the methodology described in [17] for single bridge analysis is incorporated. It should be highlighted that different boundary conditions at abutments are considered for the case of open and closed gap, while fragility curves are automatically derived for longitudinal and transverse directions separately, under the assumption of series connection between components (lower bound).

3 SEISMIC CAPACITY ASSESSMENT (LIMIT STATE THRESHOLDS)

As described in §2.1, different pier types and properties are considered, in order to develop a database encompassing practically all different types found in a bridge stock. A broad range of different section properties, namely dimensions, longitudinal and transverse reinforcement ratio, normalised axial force and material properties are considered and section analysis is performed using AnySection v.4.2.0 (as described in 2.1(b)). Damage is initially quantified using material strain values, namely ε_c and ε_s values corresponding to experimentally observed crack widths, and moment corresponding to loss of bearing capacity for limit state 4 ($M=0.9 \cdot M_{max}$). Based on cross section analysis, moment-curvature curves are calculated (bilinear curves) and curvature values corresponding to the aforementioned material strains are

defined. Hence, damage is defined in curvature terms (φ_1, φ_2, φ_3, φ_4), and M-φ curves and effective stiffnesses EI_{eff} (M_y/φ_y), needed for pushover analysis, are also defined.

Cylindrical Piers	$\varphi/D = \exp[\beta_0 + \beta_1 \cdot \ln(f_c / f_y) + \beta_2 \cdot \ln(v) + \beta_3 \cdot \ln \rho_l + \beta_4 \cdot \ln \rho_w]$ $M/2 \cdot \pi \cdot R^3 \cdot f_{cd} = \exp[\beta_0 + \beta_1 \cdot \ln(f_c / f_y) + \beta_2 \cdot \ln(v) + \beta_3 \cdot \ln \rho_l + \beta_4 \cdot \ln \rho_w]$
Hollow Cylindrical Piers	$\varphi/D_{out} = \exp[\beta_0 + \beta_1 \cdot \ln(f_c / f_y) + \beta_2 \cdot \ln(v) + \beta_3 \cdot \ln \rho_l + \beta_4 \cdot \ln \rho_w + \beta_5 \cdot \ln(D_{out}/D_{in})]$ $M/2 \cdot \pi \cdot ({R_{out}}^3 - {R_{in}}^3) \cdot f_{cd} = \exp[\beta_0 + \beta_1 \cdot \ln(f_c / f_y) + \beta_2 \cdot \ln(v) + \beta_3 \cdot \ln \rho_l + \beta_4 \cdot \ln \rho_w + \beta_5 \cdot \ln(D_{out}/D_{in})]$
Hollow Rectangular Piers (Strong Direction)	$\varphi/h = \exp[\beta_0 + \beta_1 \cdot \ln(h/b) + \beta_2 \cdot \ln(h/t) + \beta_3 \cdot \ln(v) + \beta_4 \cdot \ln(f_c / f_y) + \beta_5 \cdot \ln \rho_l + \beta_6 \cdot \ln \rho_w]$ $M/(h \cdot b - (h - 2 \cdot t) \cdot (b - 2 \cdot t)) \cdot h \cdot f_{cd} = \exp[\beta_0 + \beta_1 \cdot \ln(h/b) + \beta_2 \cdot \ln(h/t) + \beta_3 \cdot \ln(v) + \beta_4 \cdot \ln(f_c / f_y) + \beta_5 \cdot \ln \rho_l + \beta_6 \cdot \ln \rho_w]$
Hollow Rectangular Piers (Weak Direction)	$\varphi/b = \exp[\beta_0 + \beta_1 \cdot \ln(h/b) + \beta_2 \cdot \ln(h/t) + \beta_3 \cdot \ln(v) + \beta_4 \cdot \ln(f_c / f_y) + \beta_5 \cdot \ln \rho_l + \beta_6 \cdot \ln \rho_w]$ $M/(h \cdot b - (h - 2 \cdot t) \cdot (b - 2 \cdot t)) \cdot b \cdot f_{cd} = \exp[\beta_0 + \beta_1 \cdot \ln(h/b) + \beta_2 \cdot \ln(h/t) + \beta_3 \cdot \ln(v) + \beta_4 \cdot \ln(f_c / f_y) + \beta_5 \cdot \ln \rho_l + \beta_6 \cdot \ln \rho_w]$
Rectangular Piers (Strong Direction)	$\varphi/h = \exp[\beta_0 + \beta_1 \cdot \ln(b/\mathrm{h}) + \beta_2 \cdot \ln(v) + \beta_3 \cdot \ln(f_c / f_y) + \beta_4 \cdot \ln \rho_l + \beta_5 \cdot \ln \rho_w]$ $M/(h \cdot b) \cdot h \cdot f_{cd} = \exp[\beta_0 + \beta_1 \cdot \ln(\mathrm{b}/h) + \beta_2 \cdot \ln(v) + + \beta_3 \cdot \ln(f_c / f_y) + \beta_4 \cdot \ln \rho_l + \beta_5 \cdot \ln \rho_w]$
Rectangular Piers (Weak Direction)	$\varphi/b = \exp[\beta_0 + \beta_1 \cdot \ln(b/\mathrm{h}) + \beta_2 \cdot \ln(v) + \beta_3 \cdot \ln(f_c / f_y) + \beta_4 \cdot \ln \rho_l + \beta_5 \cdot \ln \rho_w]$ $M/(h \cdot b) \cdot b \cdot f_{cd} = \exp[\beta_0 + \beta_1 \cdot \ln(\mathrm{b}/h) + \beta_2 \cdot \ln(v) + + \beta_3 \cdot \ln(f_c / f_y) + \beta_4 \cdot \ln \rho_l + \beta_5 \cdot \ln \rho_w]$
Wall Piers (Strong Direction)	$\varphi/h = \exp[\beta_0 + \beta_1 \cdot \ln(b/\mathrm{h}) + \beta_2 \cdot \ln(v) + \beta_3 \cdot \ln(f_c / f_y) + \beta_4 \cdot \ln \rho_l + \beta_5 \cdot \ln \rho_w]$ $M/(h \cdot b) \cdot h \cdot f_{cd} = \exp[\beta_0 + \beta_1 \cdot \ln(\mathrm{b}/h) + \beta_2 \cdot \ln(v) + + \beta_3 \cdot \ln(f_c / f_y) + \beta_4 \cdot \ln \rho_l + \beta_5 \cdot \ln \rho_w]$
Wall Piers (Weak Direction)	$\varphi/b = \exp[\beta_0 + \beta_1 \cdot \ln(b/\mathrm{h}) + \beta_2 \cdot \ln(v) + \beta_3 \cdot \ln(f_c / f_y) + \beta_4 \cdot \ln \rho_l + \beta_5 \cdot \ln \rho_w]$ $M/(h \cdot b) \cdot b \cdot f_{cd} = \exp[\beta_0 + \beta_1 \cdot \ln(\mathrm{b}/h) + \beta_2 \cdot \ln(v) + + \beta_3 \cdot \ln(f_c / f_y) + \beta_4 \cdot \ln \rho_l + \beta_5 \cdot \ln \rho_w]$

Table 2 – Closed-form relationships for limit state thresholds of different pier types (*local* engineering demand parameter)

Section analysis results for all possible parameter combinations (nearly 8000 section analyses for each pier type considering weak and strong section axis separately), are obtained for each pier type and regression analysis is performed. Closed-form relationships for φ_y and M_y are presented in Table 2; β coefficients can be found elsewhere ([18] and online database).

The effect of varying cross section parameters on local engineering demand parameters (φ or μ_φ values) is depicted in Fig. 5 and 6 for cylindrical piers and Fig.7 for different pier types,

highlighting the over- or under-estimation of threshold values in case that a uniform value, irrespective of section properties, is considered.

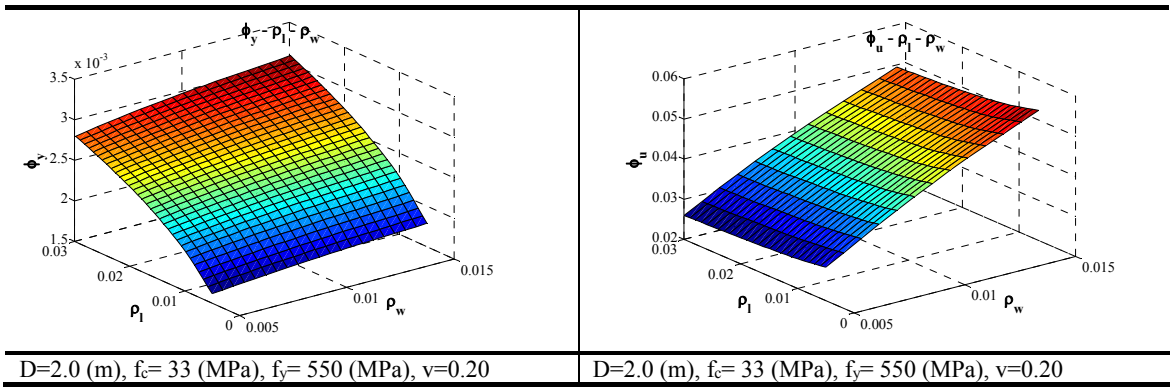

D=2.0 (m), f_c= 33 (MPa), f_y= 550 (MPa), v=0.20 | D=2.0 (m), f_c= 33 (MPa), f_y= 550 (MPa), v=0.20

Fig. 5 – Effect of longitudinal and transverse reinforcement ratio on **yield** (left) and **ultimate** (right) **curvature** of cylindrical sections

As depicted in Fig.5, yield curvature increases for increasing longitudinal reinforcement ratio (ρ_l), while the effect of transverse reinforcement ratio (ρ_w) is negligible. On the contrary, ultimate curvature is highly effected (increased) for increasing transverse reinforcement, due to the relevant increase in ultimate concrete strain (ε_{cu}) caused by core confinement, whereas the effect of concrete and steel strength on ultimate curvature is depicted in Fig. 6(right). Based on the above, curvature ductility decreases for increasing longitudinal reinforcement ratio ($\mu_\varphi=\varphi_u/\varphi_y$ – Fig. 6(left)), whereas this effect is more pronounced for ρ_l>0.01.

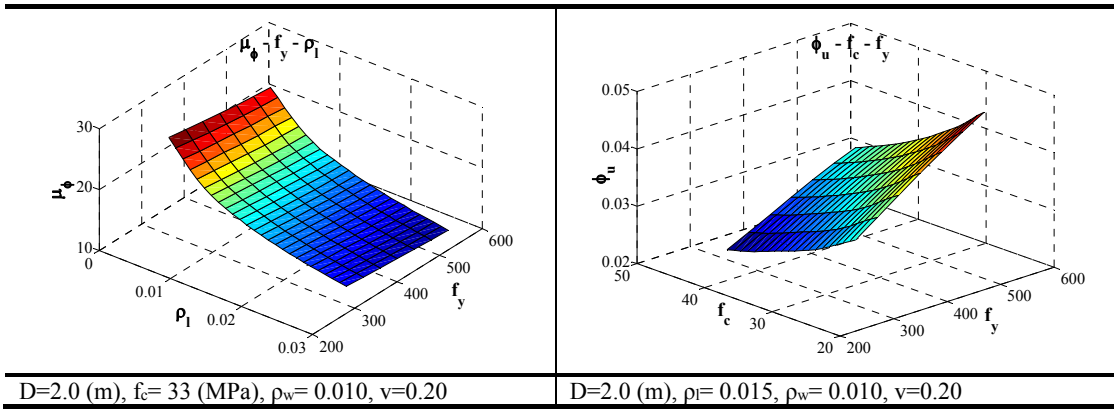

D=2.0 (m), f_c= 33 (MPa), ρ_w= 0.010, v=0.20 | D=2.0 (m), ρ_l= 0.015, ρ_w= 0.010, v=0.20

Fig. 6 – Effect of steel strength and longitudinal reinforcement ratio on **curvature ductility** (left) and steel and concrete strength on **ultimate curvature** (right) of cylindrical sections

It is evident from Fig. 7 that an increase of compressive axial load (ν_d) results in decrease of curvature ductility, due to the associated increase of compression zone depth (x_u). In addition, according to Fig. 7, the effect of transverse reinforcement increase on available curvature ductility is greater for lower values of compressive axial load.

All different pier sections considered within the database are paired with a sufficiently broad range of pier heights and pushover analyses are performed (Fig.1) to correlate local to global engineering demand parameters and quantify damage in terms of displacement of the control point (d_1, d_2, d_3, d_4). The possibility of different failure modes (flexure, shear) as well as P-delta effects are accounted for, while the number of analyses varies from 30000 to approximately 78000, depending on pier type and range of heights considered. It should be noted that various equivalent cantilever heights (e.g. equal to half the column height) should

additionally be considered, in order to account for different boundary conditions as described in §2.1(e) and Fig.1(e).

Cylindrical Piers	Hollow Rectangular Piers	Rectangular Piers
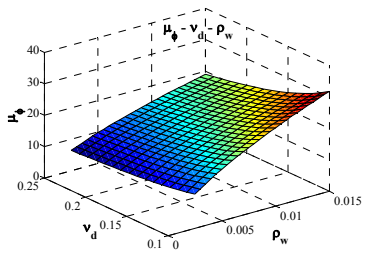	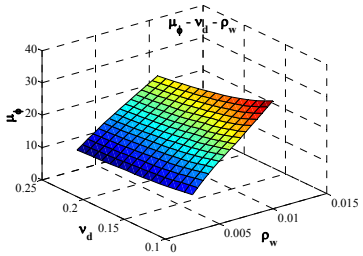	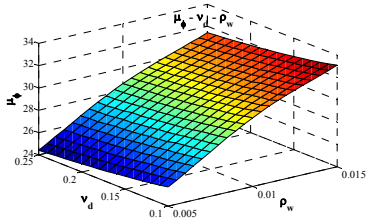
D=2.0 (m, f_c= 33 (MPa), f_y= 550 (MPa), v=0.20	H=6.0 (m), B=3.0 (m), t=0.6 (m), f_c= 33 (MPa), f_y= 550 (MPa), v=0.20	H=0.8 (m) , B=1.0 (m) , f_c= 33 (MPa), f_y= 550 (MPa), v=0.20

Fig. 7 – Effect of normalised axial force and transverse reinforcement ratio on curvature ductility of cylindrical, hollow cylindrical and rectangular sections

Cylindrical Piers	$\delta/\mathrm{H} = \exp[\beta_0 + \beta_1 \cdot \ln(\mathrm{D}/H) + \beta_2 \cdot \ln(v) + \beta_3 \cdot \ln(f_c / f_y) + \beta_4 \cdot \ln \rho_w + \beta_5 \cdot \ln \rho_l]$
Hollow Cylindrical Piers	$\delta/\mathrm{H} = \exp[\beta_0 + \beta_1 \cdot \ln(\mathrm{D}/H) + \beta_2 \cdot \ln(\mathrm{D}_{in}/\mathrm{D}_{out}) + \beta_3 \cdot \ln(v) + \beta_4 \cdot \ln(f_c / f_y) + \beta_5 \cdot \ln \rho_w + \beta_6 \cdot \ln \rho_l]$
Hollow Rectangular Piers (Strong Direction)	$\delta/\mathrm{H} = \exp[\beta_0 + \beta_1 \cdot \ln(h/H) + \beta_2 \cdot \ln(h/b) + \beta_3 \cdot \ln(h/t) + \beta_4 \cdot \ln(v) + \beta_5 \cdot \ln(f_c / f_y) + \beta_6 \cdot \ln \rho_w + \beta_7 \cdot \ln \rho_l]$
Rectangular Piers (Strong Direction)	$\delta/\mathrm{H} = \exp[\beta_0 + \beta_1 \cdot \ln(h/H) + \beta_2 \cdot \ln(b/h) + \beta_3 \cdot \ln(v) + \beta_4 \cdot \ln(f_c / f_y) + \beta_5 \cdot \ln \rho_w + \beta_6 \cdot \ln \rho_l]$
Wall Piers (Strong Direction)	$\delta/\mathrm{H} = \exp[\beta_0 + \beta_1 \cdot \ln(h/H) + \beta_2 \cdot \ln(h/b) + \beta_3 \cdot \ln(v) + \beta_4 \cdot \ln(f_c / f_y) + \beta_5 \cdot \ln \rho_w + \beta_6 \cdot \ln \rho_l]$

Table 3 – Closed-form relationships for limit state thresholds of different pier types (*global* engineering demand parameter)

Based on equivalent cantilever analysis results closed-form relationships are derived for every different pier type and limit state (d_1, d_2, d_3, d_4), as shown in Table 3. Coefficient values (β) for all pier types and both strong and weak direction can be found elsewhere ([18] and online database), whereas β values are indicatively provided for cylindrical piers and all limit states in Table 4.

Cylindrical Piers						
$\delta/\mathrm{H} = \exp[\beta_0 + \beta_1 \cdot \ln(\mathrm{D}/H) + \beta_2 \cdot \ln(v) + \beta_3 \cdot \ln(f_c / f_y) + \beta_4 \cdot \ln \rho_w + \beta_5 \cdot \ln \rho_l]$						
	β_0	β_1	β_2	β_3	β_4	β_5
δ_1/H	-6.524	-0.876	-0.018	-0.688	+0.086	+0.292
δ_2/H	-6.016	-0.674	-0.265	-0.076	+0.030	-0.072
δ_3/H	-3.872	-0.572	-0.238	-0.470	+0.505	-0.108
δ_4/H	-3.663	-0.542	-0.381	-0.518	+0.439	+0.001

Table 4 – Limit state thresholds for cylindrical piers (*global* engineering demand parameter)

The effect of varying cross section parameters on global engineering demand parameters (*d* or μ_δ values) is depicted in Fig. 8 and Fig. 9, while the conclusions are similar to those concerning local engineering demand parameters. Threshold values in terms of drift for limit state 4 increase for increasing transverse reinforcement ratio (ρ_w) due to the relative increase in ultimate curvature, while the effect of longitudinal reinforcement ratio (ρ_l) is negligible. The latter is consistent with pertinent experimental results [25]. On the contrary, regarding limit state 1, the effect of longitudinal reinforcement ratio (ρ_l) on drift value is more significant.

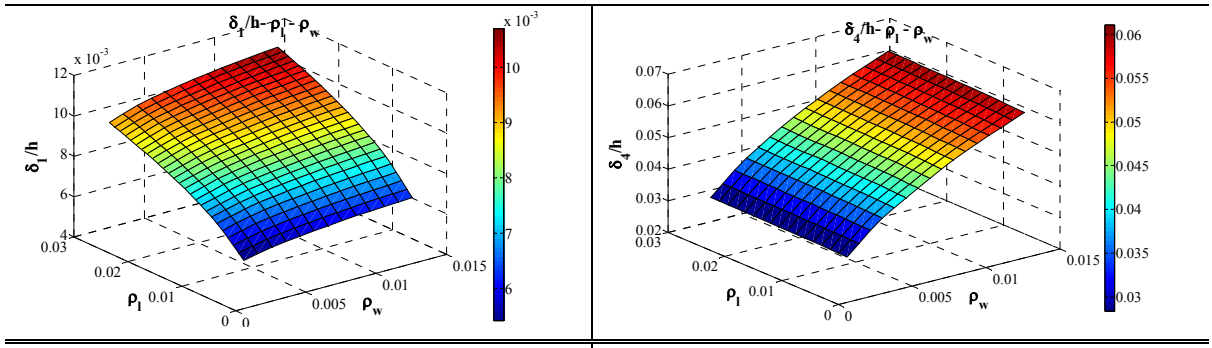

H=10 (m), D=2.0 (m), f_c= 33 (MPa), f_y= 550 (MPa), v=0.20	H=10 (m), D=2.0 (m), f_c= 33 (MPa), f_y= 550 (MPa), v=0.20

Fig. 8 –Effect of longitudinal and transverse reinforcement ratio on $\mathbf{d_1/h}$ (left) and $\mathbf{d_4/h}$ (right) value of cylindrical sections

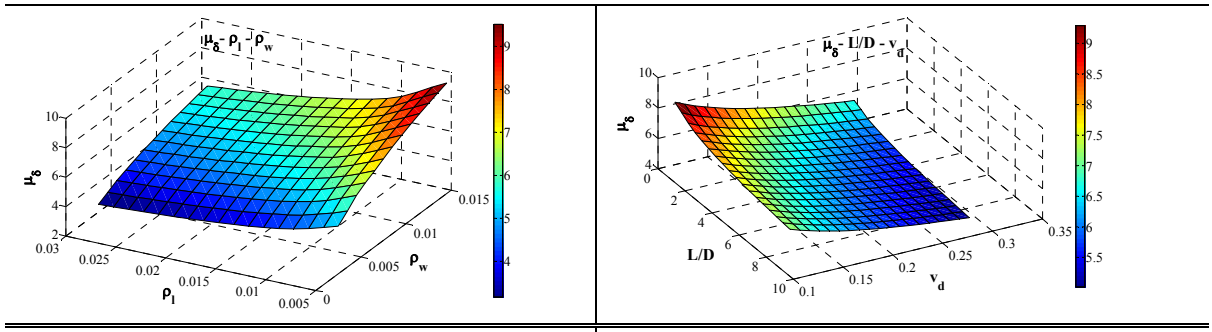

H=10 (m), D=2.0 (m), f_c= 33 (MPa), f_y= 550 (MPa), v=0.20	H=10 (m), D=2.0 (m), f_c= 33 (MPa), f_y= 550 (MPa), v=0.20

Fig. 9 – Effect of longitudinal and transverse reinforcement ratio as well as shear span and normalised axial force on displacement ductility of cylindrical piers (engineering demand parameter: μ_δ)

Displacement ductility increases for increasing transverse reinforcement ratio (ρ_w) and slightly decreases for increasing longitudinal reinforcement ratio (ρ_w) as depicted in Fig. 9 and supported by experimental results [26]. In addition, increase in compression axial load and shear span length results in decreased displacement ductility, again consistently with pertinent experimental results [27], [26].

4 SEISMIC DEMAND ASSESSMENT

4.1 Single Bridge

The calculation of seismic demand for the derivation of bridge-specific fragility curves, in the case of single bridge assessment is based on the results of nonlinear response history analysis of a detailed inelastic model. Specifically, seismic demand is calculated at the control point of every component, namely piers, bearings and abutments for different levels of earthquake intensity, using an enhanced IDA procedure described in [17] (IDA combined with

multiple stripe analysis). Multiple analyses of statistically different, yet nominally identical, bridge samples are performed and displacements of component control points are recorded and compared to limit state thresholds in order to calculate $a_{g,mean}$ for every limit state. Since lognormal distribution is assumed for the fragility curve, dispersion value, the uncertainty in seismic demand (β_D), is calculated for every component. The calculation of dispersion is computationally demanding, as it entails multiple analyses results, and could be assumed to be the same for bridges within the same category class. Three case study bridges classified to different bridge classes (according to the classification system presented in [24]) are analysed herein and uncertainty in seismic demand, additionally considering uncertainty due to record-to-record variability, is quantified. This is the most refined method for β_D quantification, based on analysis results, rather than literature recommendations [12].

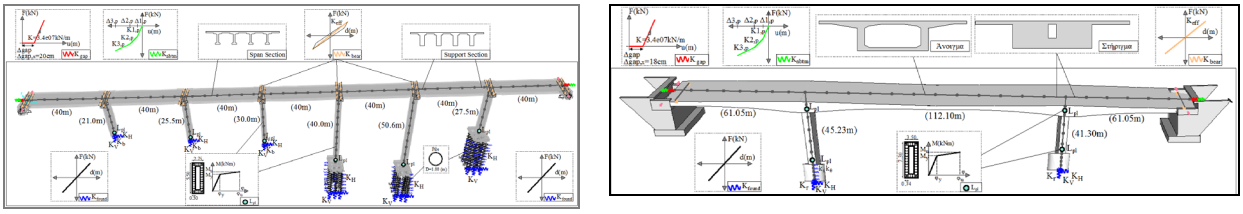

Fig. 10 – Case Studies of Egnatia Motorway Bridges (category #232(left), category #221(right))

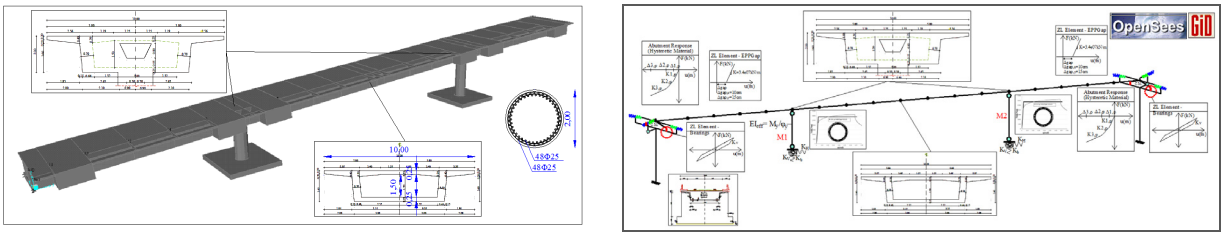

Fig. 11 – Case Study of Egnatia Motorway Bridges (category #121)

The three different case study bridges analysed herein, are typical samples of the types: simply-supported girder bridge (#232), prestressed concrete box girder bridge (#221) and overpass (#121). Uncertainty in seismic demand is calculated for different levels of earthquake intensity and all critical components and the relevant results are presented in Table 5 for #232 bridge and Fig.12 for #121 bridge. Based on the results, uncertainty in seismic demand varies, depending on the component considered and earthquake intensity. In general, uncertainty in demand increases for increased earthquake intensity, depending on the inelastic performance of the component studied. In addition, it should be highlighted that the variation of β_D values is due to record-to-record variability (three earthquake groups and different earthquake motion selection criteria for every group as described in [17]).

Longitudinal Direction											
Component	β_d (0.1g)	β_d (0.2g)	β_d (0.3g)	β_d (0.4g)	β_d (0.5g)	β_d (0.6g)	β_d (0.7g)	β_d (0.8g)	β_d (0.9g)	β_d (1.0g)	$\boldsymbol{\beta_d}$
Piers	0.45	0.44	0.46	0.82	0.81	0.81	0.85	0.89	0.87	0.86	**0.73**
Bearings	0.37	0.41	0.43	0.84	0.86	0.85	0.84	0.83	0.82	0.81	**0.71**
Abutments	--	--	0.25	0.28	0.30	0.48	0.55	0.83	0.83	0.82	**0.51**
Transverse Direction											
Component	β_d (0.1g)	β_d (0.2g)	β_d (0.3g)	β_d (0.4g)	β_d (0.5g)	β_d (0.6g)	β_d (0.7g)	β_d (0.8g)	β_d (0.9g)	β_d (1.0g)	$\boldsymbol{\beta_d}$
Piers	0.45	0.44	0.45	0.82	0.80	0.79	0.84	0.82	0.80	0.85	**0.71**
Bearings	0.44	0.42	0.42	0.84	0.85	0.84	0.79	0.78	0.77	0.77	**0.69**
Abutments	0.16	0.15	0.18	0.49	0.49	0.49	0.46	0.45	0.44	0.46	**0.38**

Table 5 – Component and system β_D values for typical simply-supported bridge (#232)

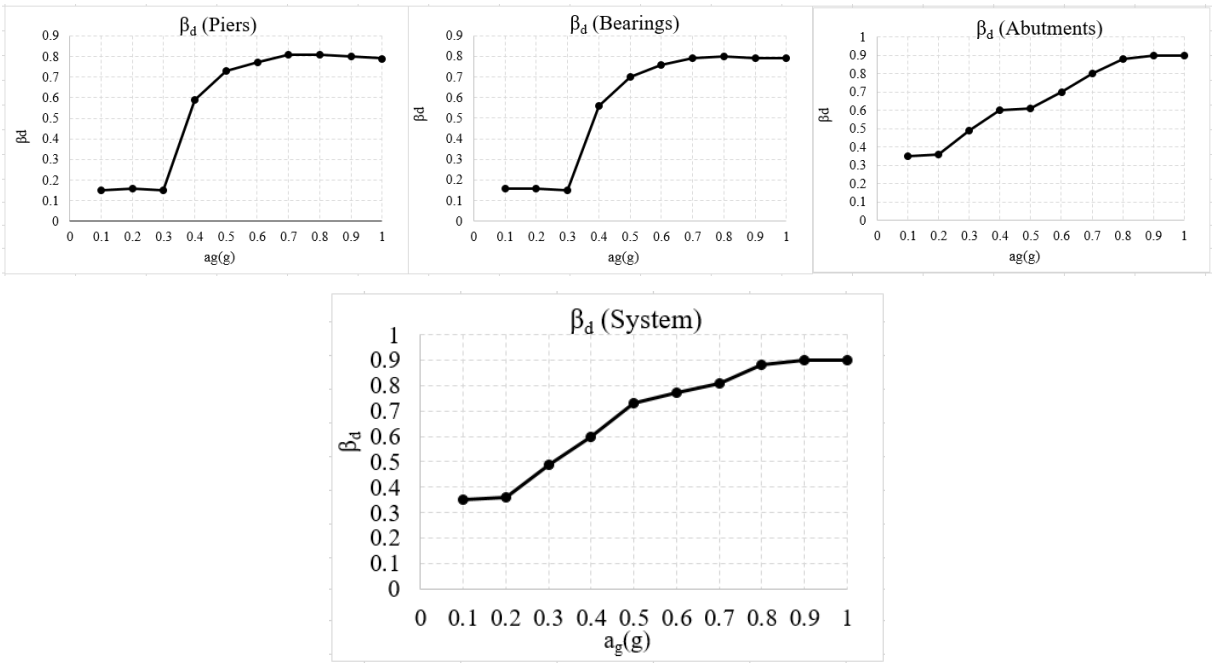

Fig. 12 – Component and system β_D values for typical overpass (#121)

4.2 Bridge stock

In the case of a bridge inventory, response spectrum analysis for varying levels of earthquake intensity is invoked, for increasing PGA values (typically from 0.1g to 1g), in order to estimate seismic demand at component control points and calculate system fragility curves for different limit states (using the Matlab-based software developed), assuming series connection between components (equation 1). Uncertainty in seismic demand (β_D value) is calculated according to §4.2 and is considered the same for bridges within the same class.

221	**Fragility (Direction x)**				**Fragility (Direction y)**						
	LS1	**LS2**	**LS3**	**LS4**	**LS1**	**LS2**	**LS3**	**LS4**	**L_{span} (m)**	**H_{pier} (m)**	**L_{tot} (m)**
1	0.35	0.68	0.86	1.33	0.30	0.75	1.19	2.02	61.5÷112.1	41.30÷45.23	234.1
2	0.30	0.76	0.83	1.07	0.48	0.70	1.21	2.38	94.5÷160	55.00÷58.00	349
3	0.36	0.93	1.23	1.74	0.54	0.77	1.36	2.58	80÷120	34.20÷36.41	290
4	0.16	0.59	0.98	1.81	0.24	0.55	0.97	1.39	75.6÷120	28.12÷63.39	636.2
5	0.33	0.79	1.12	1.33	0.41	0.77	1.36	2.58	60.75÷101.5	34÷63.03	426
6	0.24	0.89	1.13	1.39	0.45	0.70	1.17	2.40	91÷144	39÷45.10	326
7	0.36	0.72	0.95	1.35	0.35	0.77	1.34	2.32	61÷107	29.12÷87.83	457
8	0.37	0.76	0.96	1.50	0.30	0.62	1.09	2.30	64.3÷118.6	35.86÷44.89	247.2
9	0.36	0.72	0.95	1.35	0.47	0.72	0.95	2.50	85	32.47	170
10	0.29	0.75	1.04	1.80	0.43	0.62	1.09	2.32	80÷86	46.08	166
11	0.41	0.65	0.82	1.42	0.42	0.75	1.29	2.05	75÷80	38.37	155
mean	**0.32**	**0.75**	**0.99**	**1.46**	**0.40**	**0.70**	**1.18**	**2.26**			**314.23**
stand. deviation	**0.070**	**0.098**	**0.131**	**0.231**	**0.091**	**0.074**	**0.147**	**0.341**			**147.49**
COV	**22.0 %**	**13.1%**	**13.3%**	**15.8%**	**22.8%**	**10.6%**	**12.4%**	**15.1%**			**46.9%**

Table 5 – Limit state thresholds in PGA terms for all bridges of typological class #221 (longitudinal and transverse direction)

$$\max_{i=1}^{n}[\mathrm{P}(\mathrm{F}_i)] \le P(F_{system}) \le 1-\prod_{i=1}^{\pi}[1-P(F_i)] \quad (1)$$

Fragility analysis of all (44) bridges of an Egnatia motorway section (Western Macedonia, Greece) was performed using the simplified model and the results are analytically presented in [24]. Limit state thresholds in PGA terms are presented in table 5 for all (11) bridges of class #221; moreover, mean, standard deviation and coefficient of variation (COV) values based on statistical analysis of results are provided, highlighting the variation of limit state thresholds for bridges within the same category. It is seen that COV values exceed 20% in some cases, which is clearly not negligible.

5 BRIDGE-SPECIFIC AND GENERIC FRAGILITY CURVES

Based on the above, the need for a reliable methodology for bridge-specific fragility curve development is highlighted, aiming at a reliable estimation of component capacity and demand (as well as relevant uncertainty values).

The proposed methodology was applied to all bridges of categories #232 and #221 (bridges with hollow rectangular piers connected through bearings to the prestressed concrete beam deck, and monolithically connected to the box-girder bridge deck, respectively) whereas fragility curves of the generic bridge, representative of each category, are depicted in Figures 13 and 14, along with upper and lower threshold values (dashed lines - range of thresholds) for each limit state. As far as bridge class #232 is concerned, the variation of upper and lower level fragilities from the fragility curve of the generic bridge is small, therefore fragility curves of the bridge selected as representative can be used for all bridges that fall within the same category for the longitudinal direction and LS1 to LS3. The range of threshold values is fairly narrow (25% variation compared to the generic bridge) for lower limit states, however it increases for higher earthquake intensity and limit states and is dependent on the component that is critical for each limit state and the direction of loading. The variation of upper and lower level fragilities for bridge class #221 is lower for LS2 to LS4 but higher for LS1. In general, the use of the fragility curves of the generic bridge for all those in the same category may underestimate or overestimate fragility by up to 35%, however in some cases (as shown in [24] the underestimation may reach 50%.

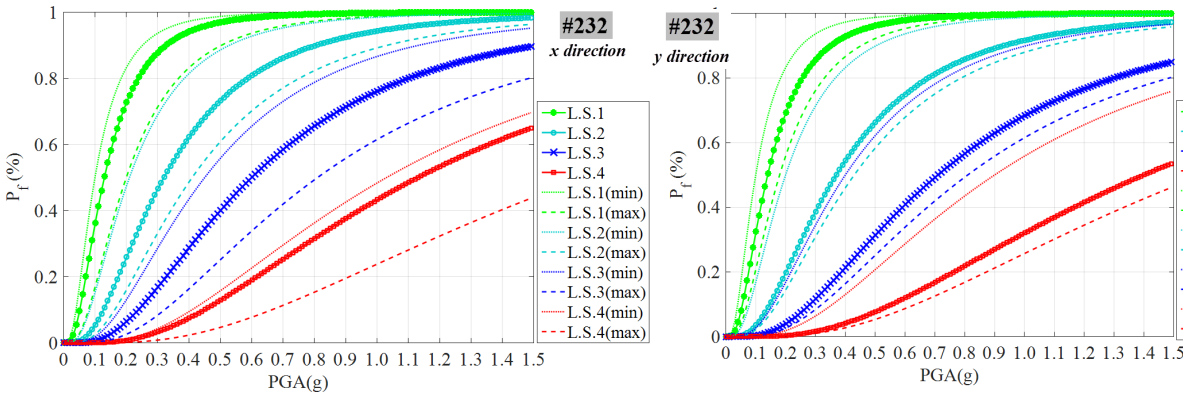

Fig. 13 – Fragility of the generic bridge in class #232 and range of damage thresholds

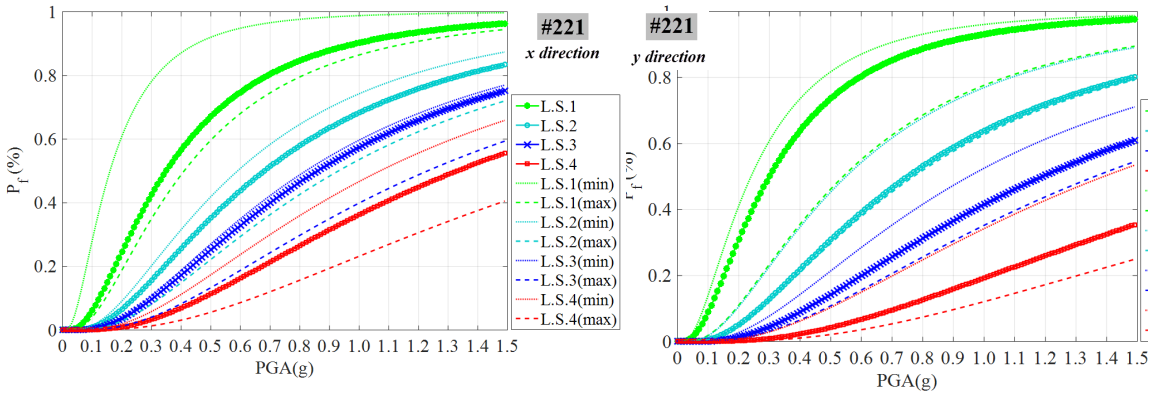

Fig. 14 – Fragility of the generic bridge in class #221 and range of damage thresholds

6 CONCLUSIONS

Capacity and demand assessment in bridge-specific fragility analysis was presented herein, in the context of developing a database for limit state thresholds (capacity estimation) and rendering computationally demanding bridge-specific analysis applicable to bridge stocks. The most important findings are summarised below:

- Limit state thresholds (capacity) are highly affected by component properties and the engineering demand parameter selected for the quantification of damage; therefore, use of component-specific values is clearly in order.
- The analysis method for the estimation of seismic demand at component control points should be differentiated according to the application scale (single bridge vs. bridge stock).
- Uncertainty in seismic demand generally increases with earthquake intensity depending on the inelastic performance of the component studied, the record-to-record variability, and the criteria for earthquake motion selection.
- The use of generic bridge fragility curves for all bridges belonging to the same category may underestimate or overestimate fragility, typically by up to 35%, however in some cases the underestimation may reach 50%, which is clearly an issue of concern. The range of LS threshold values is fairly narrow for lower limit states, but increases for higher earthquake intensity and higher limit states (heavy damage, failure).

REFERENCES

[1] Mander, J., & Basöz, N., *Enhancement of the Highway Transportation Lifeline Module in HAZUS*. Final Pre-Publication Draft (#7) prepared for National Institute of Building Sciences (NIBS), 1999

[2] Nielson, B. G., & DesRoches, R., Analytical Seismic Fragility Curves for Typical Bridges in the Central and Southeastern United States. *Earthquake Spectra*, *23*(3), 615-633, 2007(a).

[3] Cardone, D., Perrone, G., & Dolce, M., Seismic risk assessment of highway bridges. *1st US-Italy Seismic Bridge Workshop*. Pavia, Italy, 2007.

[4] Moschonas, I. F., Kappos, A. J., Panetsos, P., Papadopoulos, V., Makarios, T., & Thanopoulos, P., Seismic fragility curves for greek bridges: methodology and case

studies. *Bulletin of Earthquake Engineering*, *7*(2), 439–468, 2008.
[5] Avşar, Ö., Yakut, A., & Caner, A., Analytical Fragility Curves for Ordinary Highway Bridges in Turkey. *Earthquake Spectra*, *27*(4), 971–996, 2011.
[6] Tsionis, G., & Fardis, M. N., Seismic Fragility of Concrete Bridges with Deck Monolithically Connected to the Piers or Supported on Elastomeric Bearings. *15th World Conference of Earthquake Engineering*. Lisbon, Portugal, 2012.
[7] Choi, E., DesRoches, R., & Nielson, B., Seismic fragility of typical bridges in moderate seismic zones. *Engineering Structures*, *26*(2), 187–199, 2004.
[8] Shinozuka, M., Feng, M. Q., Lee, J., & Naganuma, T. (2000). Statistical Analysis of fragility curves. *Journal of Engineering Mechanics, ASCE*, *126*(12), 1224–1231.
[9] Cardone, D., Displacement limits and performance displacement profiles in support of direct displacement-based seismic assessment of bridges. *Earthquake Engineering & Structural Dynamics*, *43*(8), 1239–1263, 2013.
[10] Dutta, A., & Mander, J. B., Seismic fragility analysis of highway bridges. *INCEDE-MCEER Center-to-Center Workshop on Earthquake Engineering Frontiers in Transportation Systems*. Tokyo, Japan, 1998.
[11] Berry, M., & Eberhard, M., *Performance Models for Flexural Damage in Reinforced Concrete Columns*, University of Washington, 2003.
[12] *HAZUS: Earthquake loss estimation methodology.* Technical Manual, National Institute of Building for the Federal Emergency Managment Agency, Whashington, D.C., 2015.
[13] Mackie, K. R., & Stojadinović, B., R-Factor Parameterized Bridge Damage Fragility Curves. *Journal of Bridge Engineering*, *12*(4), 500–510, 2007.
[14] DesRoches, R., Padgett, J., Ramanathan, K., & Dukes, J., *Feasibility Studies for Improving Caltrans Bridge Fragility Relationships* (Vol. 0003). Georgia Institute of Technology, Atlanta, U.S.A, PhD Thesis, The State University of New York, Buffalo, 2012.
[15] Shinozuka, M., Feng, M. Q., Kim, H., & Kim, S.-H., Nonlinear Static Procedure for Fragility Curve Development. *Journal of Engineering Mechanics, ASCE*, *126*(12), 1287–1295, 2000.
[16] Nielson, B. G., & DesRoches, R., Seismic fragility methodology for highway bridges using a component level approach. *Earthquake Engineering and Structural Dynamics*, *36*, 823–839, 2007(b).
[17] Stefanidou, S. P., & Kappos, A. J., Methodology for the development of bridge-specific fragility curves. *Earthquake Engineering & Structural Dynamics*, *46*, 73–93, 2017.
[18] Stefanidou, S. P., *Structure-specific Fragility Curves for As- Built and Retrofitted Bridges*. PhD Thesis, Aristotle University of Thessaloniki (*in Greek*), 2016.
[19] Mander, J. B., Priestley, M. J. N., & Park, R., Theoretical Stress-Strain Model for Confined Concrete. *Journal Of Structural Engineering*, *114*(8), 1804–1826, 1988
[20] Priestley, M. J. N., & Ranzo, G., Seismic performance of large rc circular hollow columns. *12th World Conference of Earthquake Engineering* Auckland, New Zealand, 2000.
[21] Kappos, A. J., Analytical Prediction of the Collapse earthquake for R/C buildings : Suggested Methodology. *Earthquake Engineering & Structural Dynamics*, *20*, 167–176, 1991
[22] Papanikolaou, V. K.,Analysis of arbitrary composite sections in biaxial bending and axial load. *Computers and Structures*, *98-99*, 33–54, 2012
[23] McKeena, F., & Fenves, G. L., Open System for Earthquake Engineering Simulation. Pacific Earthquake Engineering Research Center, 2015

[24] Kappos, A. J., & Stefanidou, S. P., Importance of bridge-specific fragility curves in the seismic assessment of road networks. *16th World Conference of Earthquake Engineering*. 9-13 January, Santiago, Chile, 2017

[25] Lu, Y., Gu, X., & Guan, J., Probabilistic Drift Limits and Performance Evaluation of Reinforced Concrete Columns. *Journal of Structural Engineering*, *131*(6), 966–978., 2005.

[26] Lee, J.-H., Choi, J.-H., Hwang, D.-K., & Kwahk, I.-J., Seismic performance of circular hollow RC Bridge columns. *KSCE Journal of Civil Engineering*, *1-12*, 2014.

[27] Erduran, E., & Yakut, A., Drift based damage functions for reinforced concrete columns. *Computers & Structures*, *82*, 121–130, 2004.